

Cite this: *Chem. Sci.*, 2023, 14, 5899

All publication charges for this article have been paid for by the Royal Society of Chemistry

## Role and dynamics of transition metal carbides in methane coupling†

Seraphine B. X. Y. Zhang,<sup>a</sup> Quentin Pessemesse,<sup>b</sup> Lukas Lätsch,<sup>a</sup> Konstantin M. Engel,<sup>a</sup> Wendelin J. Stark,<sup>a</sup> Alexander P. van Bavel,<sup>c</sup> Andrew D. Horton,<sup>c</sup> Pierre-Adrien Payard<sup>b,\*</sup> and Christophe Copéret<sup>a,\*</sup>

Transition metal carbides have numerous applications and are known to excel in terms of hardness, thermal stability and conductivity. In particular, the Pt-like behavior of Mo and W carbides has led to the popularization of metal carbides in catalysis, ranging from electrochemically-driven reactions to thermal methane coupling. Herein, we show the active participation of carbidic carbon in the formation of C<sub>2</sub> products during methane coupling at high temperature that is associated with the dynamics of Mo and W carbides. A detailed mechanistic study reveals that the catalyst performance of these metal carbides can be traced back to its carbon diffusivity and exchange capability upon interaction with methane (gas phase carbon). A stable C<sub>2</sub> selectivity over time on stream for Mo carbide (Mo<sub>2</sub>C) can be rationalized by fast carbon diffusion dynamics, while W carbide (WC) shows loss of selectivity due to slow diffusion leading to surface carbon depletion. This finding showcases that the bulk carbidic carbon of the catalyst plays a crucial role and that the metal carbide is not only responsible for methyl radical formation. Overall, this study evidences the presence of a carbon equivalent to the Mars–Van Krevelen type mechanism for non-oxidative coupling of methane.

Received 25th February 2023  
Accepted 2nd May 2023

DOI: 10.1039/d3sc01054f

rsc.li/chemical-science

## Introduction

Transition metal carbides<sup>1</sup> are ubiquitous in catalysis today, particularly in the context of C–H activation.<sup>2–8,28</sup> While molybdenum and tungsten are prominent metals in state-of-the-art catalysts for oxidative and non-oxidative coupling of methane,<sup>9,10</sup> MoO<sub>x</sub>/ZSM-5 has become the gold standard for methane coupling to aromatics.<sup>9,11</sup> For this system a characteristic induction period along with particle agglomeration is observed which is rationalized by a transformation of the molybdenum oxide to the corresponding oxycarbide or carbide species which is presumed to resemble the active species in methane coupling.<sup>12,13,27,29,30</sup> Yet, the mechanism for non-oxidative coupling of methane is still a matter of debate. High reaction temperatures, *i.e.* in the range of 800–1100 °C, suggest the involvement of radical pathways in the gas phase and the catalyst activity is often ascribed to methyl radical formation which then couple to C<sub>2</sub> products

downstream of the catalyst bed.<sup>14,15,31</sup> Previous reports addressing the involvement of carbidic carbon in metal carbide catalysts<sup>16,17,32</sup> prompted us to investigate the role of carbon closer in bulk Mo and W carbides (Mo<sub>2</sub>C and WC) by applying a <sup>13</sup>C-labelling strategy combined with several spectroscopic techniques (XPS, ss-NMR, pXRD) and metadynamics simulations. Mo and W carbides were tested as catalysts for the non-oxidative coupling of methane (NOCM). Both materials enable C<sub>2</sub> product formation at 1100 °C with 21% C<sub>2</sub> selectivity at 23% CH<sub>4</sub> conversion for Mo<sub>2</sub>C (4.7% C<sub>2</sub> yield) and 32% C<sub>2</sub> selectivity at 10% CH<sub>4</sub> conversion for WC (3.2% C<sub>2</sub> yield). Furthermore, this study shows that carbidic carbon participates in C<sub>2</sub> product formation and interacts with methane (gas phase carbon). Differences in methane coupling activity could be rationalized by investigating surface composition with XPS and carbon diffusion coefficients by metadynamics at the DFT level. Following the analysis, we concluded fast C exchange dynamics for Mo<sub>2</sub>C and slow C diffusion for WC. The incorporation of carbon originating from methane was evidenced by ss-NMR of the spent materials with carbidic carbon NMR signatures at 274 ppm and 307 ppm for Mo<sub>2</sub>C and WC, respectively. Hence, this study reveals the presence of a carbon equivalent to the Mars–Van Krevelen mechanism in non-oxidative coupling of methane, which is typically encountered in oxidation processes with certain metal oxides.<sup>18,19</sup>

<sup>a</sup>Department of Chemistry and Applied Biosciences, ETH Zurich, Vladimir-Prelog-Weg 1–5, 8093 Zürich, Switzerland. E-mail: ccoperet@ethz.ch

<sup>b</sup>Université de Lyon, Université Claude Bernard Lyon I, CNRS, INSA, CPE, UMR 5246, ICBMS, 1 rue Victor Grignard, 69622 Lyon, France. E-mail: pierre-adrien.payard@univ-lyon1.fr

<sup>c</sup>Shell Global Solutions International B. V., Grasweg 31, 1031 HW Amsterdam, Netherlands

† Electronic supplementary information (ESI) available. See DOI: <https://doi.org/10.1039/d3sc01054f>

## Results and discussion

### Synthesis and activity of transition metal carbides

Mo<sub>2</sub>C and WC were prepared *via* carburization at 1000 °C, and their catalytic activity in NOCM was investigated (Fig. 1). They were characterized with pXRD, XPS and TEM. Detailed synthesis procedures, characterization and catalytic test conditions for Mo<sub>2</sub>C and WC can be found in the ESI.†

Unless otherwise stated, all data sets are averages of 1-hour time on stream (TOS) at a given temperature. At 1100 °C, Mo<sub>2</sub>C and WC convert methane to C<sub>2</sub> products and coke with C<sub>2</sub> yields of 4.7% for Mo<sub>2</sub>C and 3.2% for WC (Fig. 1a). For Mo<sub>2</sub>C, methane conversion increases with temperature: from 9.7% at 900 °C to values of up to 23.0% at 1100 °C with an average C<sub>2</sub> selectivity of 20.6% which is stable over time on stream. In the case of WC, methane conversion reaches a maximum of 9.9% at 1100 °C with a C<sub>2</sub> selectivity of 32.5%, while a loss of selectivity is observed over time on stream. Comparing both carbides, methane conversion is higher for Mo<sub>2</sub>C while the C<sub>2</sub> selectivity is higher for WC. It is also noteworthy that at 900 °C WC already converts methane, albeit with a low C<sub>2</sub> selectivity of 3.2% while

no C<sub>2</sub> products are detected for Mo<sub>2</sub>C. The best selectivity towards C<sub>2</sub> products between the two catalysts was determined as 32.5% at 9.9% methane conversion for WC at 1100 °C, albeit the latter suffers from a fast deactivation.

In general, the highest conversion levels and C<sub>2</sub> selectivities are obtained at high temperatures (Fig. 1b). Mo<sub>2</sub>C on the one hand exhibits stable selectivity at increasing conversion during time on stream at 1100 °C, forming coke and aromatics as major reaction byproducts (Fig. 1c). WC on the other hand experiences rapid loss of C<sub>2</sub> selectivity over time on stream at 1100 °C along with increasing methane conversion (Fig. 1d).

### Role of carbon in Mo and W carbides

The evolution of Mo<sub>2</sub>C and WC materials was furthermore investigated by comparing the materials before and after NOCM (3 h on stream at 900, 1000 and 1100 °C, 1 h at each temperature) using pXRD and XPS (Fig. 2). Based on pXRD, the bulk structures of Mo and W carbide remain unchanged for pristine and spent catalysts. XPS gives insight regarding differences in surface composition, namely carbon (surface) depletion for WC and structural retention for Mo<sub>2</sub>C. In the case of Mo<sub>2</sub>C, two

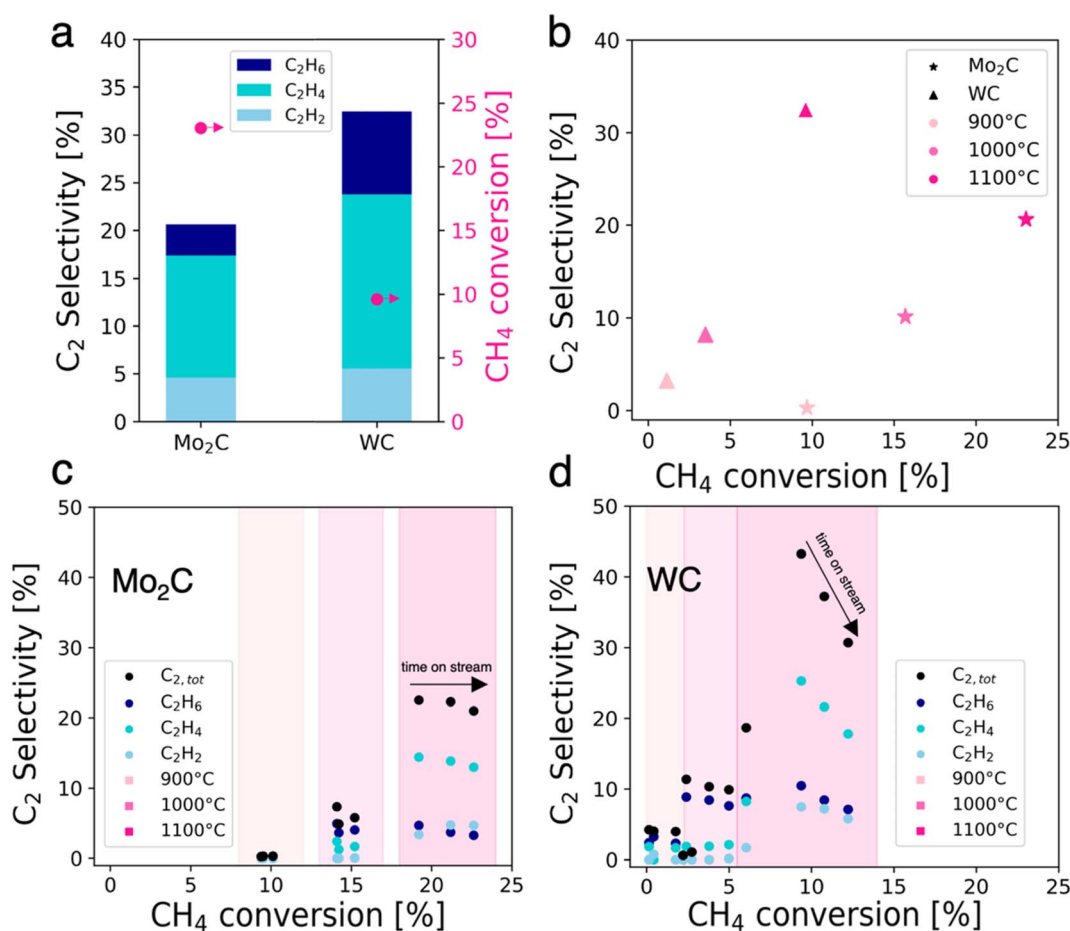


**Fig. 1** (a) Selectivity distribution for C<sub>2</sub> species and CH<sub>4</sub> conversion at 1100 °C with 10% CH<sub>4</sub> in argon for Mo<sub>2</sub>C and WC (averaged over 1 h time on stream). (b) Effect of reaction temperatures on the C<sub>2</sub> selectivity and CH<sub>4</sub> conversion for the different catalysts. The color indicates the temperature and the form the catalyst. CH<sub>4</sub> conversion vs. C<sub>2</sub> selectivity at 900, 1000 and 1100 °C for C<sub>2</sub> species over time on stream for (c) Mo<sub>2</sub>C and (d) WC; data points were taken every 15 min.

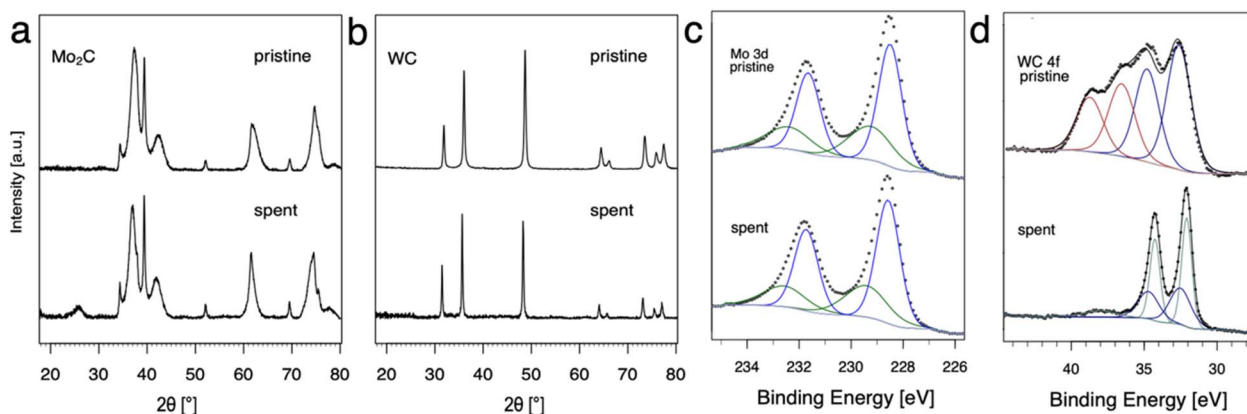


Fig. 2 Structural transformations for pristine and spent catalyst materials are shown. pXRD for (a)  $\text{Mo}_2\text{C}$ , (b) WC and XPS spectra of pristine and spent metal carbides: (c)  $\text{Mo}_2\text{C}$  3d, (d) WC 4f. The dots represent the recorded data and the solid lines show the results of a curve-fitting procedure.

components of the  $3d_{5/2}$  peak are observed at binding energies of 228.6 and 229.4 eV associated with  $\text{Mo}^{2+}$  ( $\text{Mo}_2\text{C}$ ) and  $\text{Mo}^{4+}$  ( $\text{MoC}$  or  $\text{MoO}_2$ ), respectively.<sup>12,20,29</sup>

This finding remains unchanged considering pristine and spent catalyst surface. For WC, the XPS spectra (Fig. 3d) can be fitted as two multiplets that correspond to the  $\text{W } 4f_{7/2}$  and  $\text{W } 4f_{5/2}$  components which have a spin-orbit splitting of 2.2 eV. The WC ( $\text{W}^{4+}$ ) peaks were identified at 32.5 and 32.7 eV for the pristine and the spent catalyst, respectively. The  $\text{W } 4f_{7/2}$  peak at 36.6 eV was attributed to  $\text{WO}_3$ . Pristine WC shows a mixture of WC (32.5 eV) and  $\text{WO}_3$  (36.6 eV) on the surface. While no  $\text{WO}_3$  was found in the spent WC, reduction to metallic  $\text{W}(0)$  with the  $4f_{7/2}$  component at 32.1 eV was observed. For  $\text{W}(0)$  metal, a characteristic loss feature is reported, here it can be observed as a broad peak at 38 eV.<sup>21</sup> Overall, XPS measurements show

a change in composition for the surface from a mixture of  $\text{WO}_3$  and WC in the pristine catalyst to WC and  $\text{W}(0)$  in the spent catalyst hinting towards carbon depletion on the surface of WC with concomitant reduction to metallic W.

Intrigued by this finding, the reaction of  $^{13}\text{CH}_4$  with these materials was investigated in order to elucidate the role of surface C in transition metal carbides and to examine whether there is incorporation of the carbide surface C in the final products.  $^{13}\text{CH}_4$  labelling experiments were performed for  $\text{Mo}_2\text{C}$  and WC in a batch reactor (see Fig. S10†). The reactor was filled with the respective metal carbide, 200 mbar of  $^{13}\text{CH}_4$  at r.t., heated to 1100 °C with a heating ramp of 400 °C  $\text{h}^{-1}$  and subsequent aliquots were taken after 3, 6, 9 and 12 h. Aliquots of the gas mixture are taken and analyzed with GCMS resulting in mass fragmentation patterns allowing to monitor the

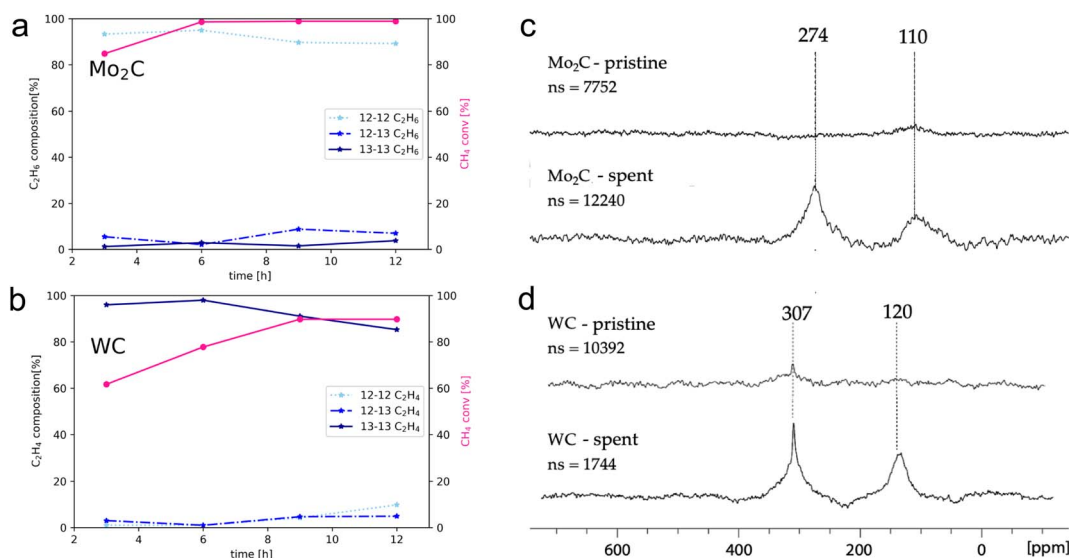


Fig. 3 Left: Product distribution for dilabelled, monolabelled and non-labelled  $\text{C}_2$  products in case of  $\text{Mo}_2\text{C}$  (a) and WC (b) as a function of contact time. Right:  $^{13}\text{C}$  MAS NMR characterization of pristine and spent (c)  $\text{Mo}_2\text{C}$  and (d) WC. The catalyst was contacted with 200 mbar  $^{13}\text{CH}_4$  (at r.t.) in batch for 24 h at 1100 °C (molar ratio 7.2 WC: 1  $^{13}\text{CH}_4$  and 6.9  $\text{Mo}_2\text{C}$ : 1  $^{13}\text{CH}_4$ ).

distribution of isotopomers among coupling products (non-, mono- and di-labelled  $C_2$  products) for ethane, ethylene and acetylene (see Table S2 and Fig. S7†).

The degree of carbidic  $^{12}C$  incorporation into  $C_2$  products was investigated by monitoring product evolution over the course of 12 h, with aliquots drawn every 3 h (Fig. 3a and b).

In the case of  $Mo_2C$ , the isotopomer distribution is dominated by non-labelled  $C_2$  products, with ethane and ethylene as major gaseous products. The isotopomer distribution among ethane (Fig. 3a) is dominated by the non-labelled  $C_2H_6$  (93%) after 3 hours, with mono- and di-labelled  $C_2H_6$  being at 6% and 1%, respectively. The ratios of isotopomers change slightly with time; the amount of non-labelled  $C_2H_6$  reaches 89% along with 7 and 4% of mono- and di-labelled isotopomers after 12 h. This finding suggests the incorporation of carbidic carbon in  $C_2$  products and C mobility in the  $Mo_2C$  matrix. Considering that the surface and the bulk of  $Mo_2C$  remains unchanged according to XPS and pXRD analysis, this labelling study further suggests fast C exchange with gas phase  $^{13}CH_4$  resulting in rapid reformation of the  $Mo_2C$  and thus allows for maintaining a constant product selectivity. The exchanged carbidic C is replenished with  $^{13}C$  from the gas phase explaining the increase in labelled products over time.

For WC (Fig. 3b), ethylene is formed as major gaseous product under the same reaction conditions. However, in sharp contrast to  $Mo_2C$ , the amount of di-labelled  $C_2H_4$  isotopomer dominates (97%) for WC, with only a minor fraction of non- (1%) and mono-labelled (2%)  $C_2H_4$  after 3 h. With increasing reaction time and conversion of  $^{13}CH_4$ , the relative amount of  $^{12}C$  isotopomer increases with mono- and non-labelled isotopomers  $C_2H_4$  reaching 14% and 9%, respectively after 12 h, indicating that WC can also act as a source of carbon, albeit much less efficiently than  $Mo_2C$ . As discussed above, this process is accompanied by a reduction over time of WC to W(0) as evidenced by XPS (Fig. 2d), indicating a C depletion of the WC matrix. This change in catalyst state and the presence of metallic W offers a possible explanation for the loss of selectivity over time on stream with simultaneous increase in methane conversion. Considering the sharp contrast of reactivity patterns in these carbides (observed in the presence of labelled methane), one might pose the question whether  $Mo_2C$  and WC can release carbon in the form of methane by interaction with  $H_2$  (10%  $H_2$  in Ar, 40 mL  $min^{-1}$ , up to 1100 °C). As expected from their different carbon mobility (*vide infra*), methane evolution could only be observed for  $Mo_2C$  (see Fig. S23†). In order to study  $^{13}C$  enrichment in the spent materials by exchange between the surface  $^{12}C$  of the carbide and the gas phase  $^{13}CH_4$ , the materials were further examined by  $^{13}C$  MAS NMR (Fig. 3c and d). It should be noted that good quality spectra could only be obtained when diluting the sample with KBr. While hardly any signal is observed on pristine materials, in particular for  $Mo_2C$ , intense signals are observed post-reaction, consistent with the exchange of carbon between the gas phase and the solid, thereby confirming enrichment of the spent catalyst with  $^{13}C$ . For both WC and  $Mo_2C$ , two peaks are observed, corresponding to the carbidic carbon and  $sp^2$  carbon signals (graphitic carbon), the former

appearing at 307 ppm for WC and at 274 ppm for  $Mo_2C$ . The  $^{13}C$  shift of  $Mo_2C$  agrees with previous reports,<sup>27</sup> while the spectrum of WC has to date not been reported to the best of our knowledge.

One may note that the  $sp^2$  carbons have different chemical shifts for WC and  $Mo_2C$ , indicating the presence of different types of carbons, possibly aromatic carbon deposit around 120 ppm vs. graphitic carbon around 110 ppm for WC and  $Mo_2C$ , respectively.<sup>22,23</sup> Summarizing these findings, the incorporation of surface/carbidic  $^{12}C$  from the carbide in the  $C_2$  products was shown for both  $Mo_2C$  and WC, yet  $Mo_2C$  exhibits a significantly higher C mobility of the carbide matrix than WC. The faster exchange/diffusion of carbidic carbon or the formation of methane from  $Mo_2C$  are possible rationales for these contrasting isotopomer distributions.

### Modelling diffusion of carbon in $Mo_2C$ and WC

In order to better understand the carbon exchange capability of molybdenum and tungsten carbides, the diffusion mechanism of carbon in the matrix at 1100 °C was explored using metadynamics at the DFT level (see the computational details for the method used).<sup>24,25,33–35</sup> The diffusion of a single carbon atom through a periodic cell of the two most stable carbide stoichiometries  $Mo_2C$  and WC was investigated. The (001), (010) and (011) facets were considered to account for the anisotropy of the material; diffusion mechanisms and diffusion coefficients were similar in all cases so that only the (010) case will be discussed in the following, see ESI Section 7† for facets (001) and (011) and computational details. The cells consist of 6-atom layers with two fixed bottom layers. A potential bias was applied along selected collective variables, namely: the vertical position of the C atom ( $z$ ), the C–C and C–M coordination numbers,  $N_{coord}(C-C)$  and  $N_{coord}(C-M)$  respectively, to accelerate diffusion. The free energy surfaces associated to  $z$  and  $N_{coord}(C-C)$  were reconstructed by summing up the energy bias. The calculated free energy barrier (Fig. 4c, from  $z = 0.5 \text{ \AA}$  to  $z = 5.5 \text{ \AA}$ ) to diffuse from the resting site to a higher lying site in  $Mo_2C$  is  $\sim 40 \text{ kcal mol}^{-1}$ , which corresponds to a diffusion coefficient of  $D_{Mo_2C}^{1373K} = 1.3 \times 10^{-11} \text{ m}^2 \text{ s}^{-1}$  at 1100 °C. This value suggests that carbon diffuses easily in the bulk at this temperature with an order of magnitude of the diffusion coefficient similar to the one obtained at ambient temperature for organic molecules in a liquid phase.<sup>26</sup> The carbon diffusion in  $Mo_2C$  takes place through migration of a C atom from a resting octahedral site ( $O_h$ ) to vacant tetrahedral ( $T_d$ ) ones (Fig. 4a). As evidenced by the variation of the collective variables with time (Fig. 4b), two different tetrahedral sites are present in the crystal structure leading either to an isolated tetrahedral carbide ( $N_{coord}(C-C) = 0$ , Fig. 4a,  $Td(C_0)$ ) or to the formation of a  $C_2$  moiety with an adjacent octahedral C neighbor ( $N_{coord}(C-C) = 1$ , Fig. 4a,  $Td(C_1)$ ). In the latter, distortion of the crystal structure may lead to the formation of  $C_2$  defects with neighboring carbon sites, slowing down migration through these sites. As indicated by the free energy surface (FES, Fig. 4c,  $N_{coord}(C-C) = 1$ ),  $C_2$  defects are easily formed at this temperature and are likely to be involved in the subsequent formation of the coupling products. The





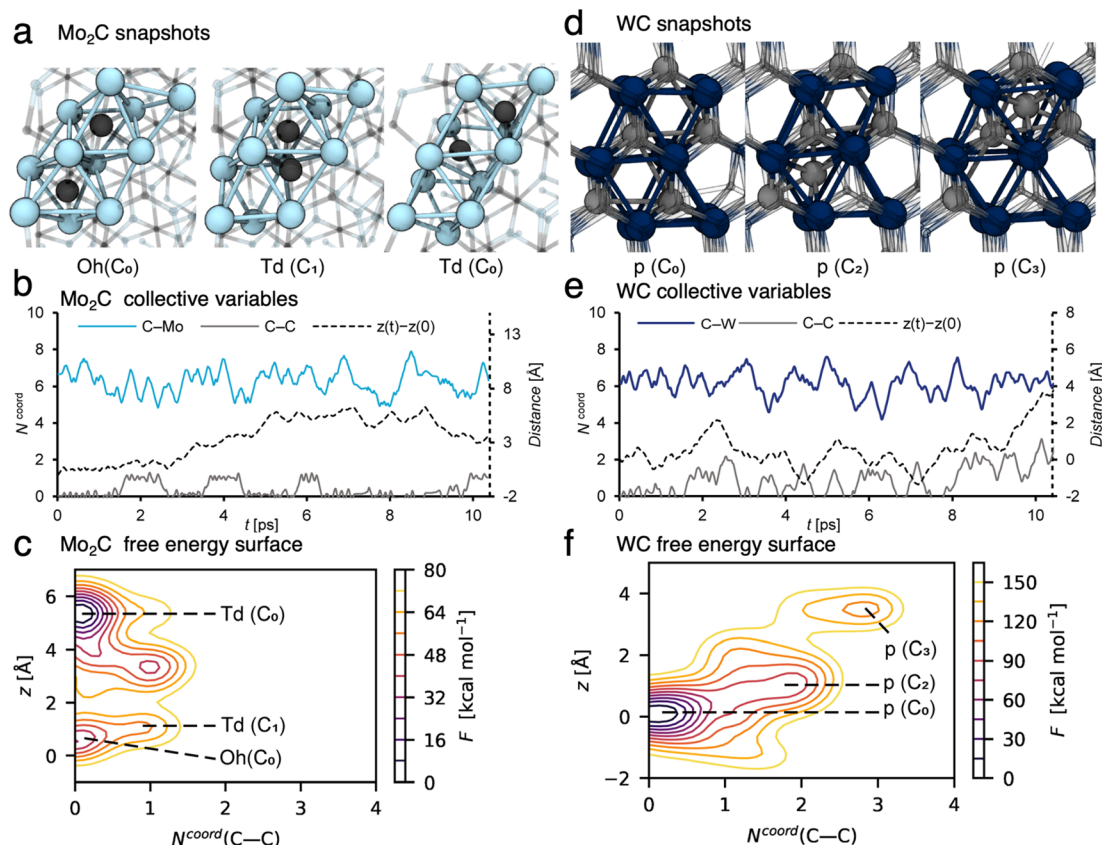


Fig. 4 Successive sites involved in the diffusion of carbon towards the (010) facet in  $\text{Mo}_2\text{C}$  ((a) octahedral  $\text{O}_h$  and tetrahedral  $\text{T}_d$  sites with  $(\text{C}_1)$  or without C–C interaction ( $\text{C}_0$ )) and WC ((d) prismatic sites  $p$  with  $x$  C neighbors  $\text{C}_x$ ). Biased collective variables as a function of the simulation time for the diffusion of carbon in  $\text{Mo}_2\text{C}$  (b) and in WC (e). Free-energy surfaces as a function of the coordination number from C to C ( $N_{\text{coord}}(\text{C}–\text{C})$ ) and distance along the  $z$  axis with respect to the initial position ( $z$ ) for  $\text{Mo}_2\text{C}$  (c) and WC (f).

contrasting behavior for WC reoccurs as the calculated diffusion of carbide carbon in WC is significantly slower. The calculated free energy barrier for diffusion in WC (Fig. 4f between  $z = 0$  Å and  $z = 4$  Å) and the associated diffusion coefficient are  $\sim 140$  kcal mol $^{-1}$  and  $D_{\text{WC}}^{1373\text{K}} = 7.5 \times 10^{-30}$  m $^2$  s $^{-1}$ , respectively.

For WC, carbon has to move through surrounding unoccupied prismatic sites (Fig. 4d,  $p(\text{C}_2)$  and  $p(\text{C}_3)$ ), and interacts with the carbon atoms occupying the neighboring prismatic sites (Fig. 4e,  $N_{\text{coord}}(\text{C}–\text{C}) > 0$ ), leading to the formation of transient  $\text{C}_x$  moieties ( $x = 3$  and  $4$ , Fig. 4e and f). The difference in calculated diffusion coefficients of around 20 orders of magnitude between  $\text{Mo}_2\text{C}$  and WC is in agreement with the distribution of  $\text{C}_2$  products, which contain mainly non-labelled species originating from the  $^{12}\text{C}$ -bulk in the case of  $\text{Mo}_2\text{C}$ , and mainly di-labelled species originating from the  $^{13}\text{CH}_4$  reactant gas in the case of WC. These results further confirm what was observed by XPS (*vide supra*). In WC, carbon diffusion is slow and carbon depletion is not compensated by incorporation of carbon from gas phase methane, thus leading to formation of metallic  $\text{W}(0)$ . In the case of  $\text{Mo}_2\text{C}$ , carbon easily diffuses through the bulk and is replenished rapidly at the surface as the spent catalyst's XPS signature resembles the pristine one.

## Conclusions

In this study, the crucial role of carbide carbon in the active catalytic materials was shown by (i) incorporation of carbide carbon in  $\text{C}_2$  products, (ii) reduction of WC to  $\text{W}(0)$  leading to a loss of product selectivity, (iii)  $^{13}\text{C}$  exchange between gaseous methane and Mo/W carbide surfaces as evidenced by ss-NMR and (iv) computation of carbon diffusion coefficients in Mo and W carbides. Based on the incorporation of carbon from the bulk in the  $\text{C}_2$  products, a Mars–Van Krevelen type mechanism<sup>19</sup> with participation of carbide carbon of the metal carbide (instead of oxygen in a metal oxide) is most suited to rationalize our findings. This observation parallels what has been proposed in the Fischer-Tropsch process based on Fe carbide<sup>36</sup> or for the methane aromatization on  $\text{MoO}_x$  and  $\text{WC}_x$  clusters on ZSM-5.<sup>17,37</sup>

For  $\text{Mo}_2\text{C}$ , fast carbon diffusion, as shown by labelling studies and computations, allows replenishment of the surface and a good catalytic performance (stable selectivity). In sharp contrast, under the same conditions, WC undergoes reduction of the surface species to  $\text{W}(0)$ , consistent with the significantly lower fraction of carbide carbon incorporated into the gaseous products and the slower calculated carbon diffusion, probably explaining the fast loss of  $\text{C}_2$  product selectivity.



For carbides with higher carbon diffusion coefficients like Mo<sub>2</sub>C, two carbidic carbons can recombine to form a C<sub>2</sub> unit and desorb by combining with hydrogen atoms adsorbed on the surface; this would explain the absence of labelling of the hydrocarbon products at the initial stage, the labelling of the carbide without its reduction and the incorporation of <sup>13</sup>C with increasing time.

With decreasing carbon mobility like for WC, the formation of products involves surface reactions, where C–H activation can form surface hydrocarbyls (alkyl, alkylidene and alkylidines) as previously proposed.<sup>38,39</sup>

CH<sub>x</sub> species on the surface can then recombine and desorb as C<sub>2</sub> unit or can interact with a non-labelled surface C releasing a mono-labelled C<sub>2</sub> product facilitated by H<sub>ads</sub>, as previously proposed.<sup>38,40,41</sup> In the propagation of the catalytic process, the carbidic carbon on the surface can be regenerated by diffusion through the bulk or by interaction with methane in the gas phase. While above-described pathways might be more pronounced for certain metal carbides, it is most likely a combination thereof.

This study supports that a Mars–van Krevelen-like mechanism involving carbon atoms is at play, paralleling what is observed with oxygen and metal oxides in several oxidation reactions.<sup>16,27,32</sup> While more insights in the mechanism of methane coupling are certainly needed to fully understand the product formation processes, this work shows that carbidic carbon and its dynamic behavior play a crucial role in methane coupling to higher hydrocarbon products; governing selectivity and conversion. It is further highlighted here that dynamics of metal carbides should be considered more broadly and integrated as design parameters in catalysis.

## Data availability

All data are available upon request.

## Author contributions

S. B. X. Y. Z. performed all experiments and catalytic tests, measured pXRD, XPS, was involved in the development of the computational method and led the writing process. Q. P. performed metadynamics simulations under guidance of P.-A. P. L. L. measured NMR. K. E. synthesized WO<sub>3</sub>. All authors contributed to data interpretation and writing.

## Conflicts of interest

The authors declare no competing interests.

## Acknowledgements

We thank Shell Global Solution International B. V. for financial support. We thank Dennis Roelofszen (Shell) for consulting on technical details. Dr Nicolas Kaeffer (MPI CEC) and Dr Sourav Chatterjee (ETHZ) are acknowledged for fruitful discussions. Giovanni Cossu (ETHZ) is acknowledged for discussions and support regarding XPS. We thank the Mougel group (ETHZ) for

access to XPS measurements. This work was carried out in part within the NCCR catalysis (financial support to the Stark group). P.-A. Payard and Q. Pessemeesse are grateful to the Ecole Normale Supérieure de Lyon, Université Lyon 1 and the Region Auvergne Rhone Alpes for financial support and would like to thank Dr M.-E. L. Perrin (Univ Lyon) for precious advice and discussion. P.-A. P. and Q. P. are grateful to the CCIR of ICBMS, PSMN, GENCI-TGCC (Grants A0100812501 and A0120813435) for providing computational resources and technical support.

## Notes and references

- 1 H. H. Hwu and J. G. Chen, *Chem. Rev.*, 2005, **105**, 185–212.
- 2 R. B. Levy and M. Boudart, *Science*, 1973, **181**, 547–549.
- 3 Y. Deng, Y. Ge, M. Xu, Q. Yu, D. Xiao, S. Yao and D. Ma, *Acc. Chem. Res.*, 2019, **52**(12), 3372–3383.
- 4 B. Anasori, M. R. Lukatskaya and Y. Gogotsi, *Nat. Rev. Mater.*, 2017, **2**, 16098.
- 5 Z.-T. Xiong, L.-L. Chen, H.-B. Zhang, J.-L. Zeng and G.-D. Lin, *Catal. Lett.*, 2001, **74**, 227–232.
- 6 G. K. Dixit, M. Kumar, A. Katiyar, A. P. Jansen, A. P. van Bavel, R. Agrawal, P. M. Shenai and V. Srinivasan, *Catal. Sci. Technol.*, 2021, **11**, 7398–7411.
- 7 C. Geng, T. Weiske, J. Li, S. Shaik and H. Schwarz, *J. Am. Chem. Soc.*, 2019, **141**, 599–610.
- 8 S. T. Hunt, M. Milina, A. C. Alba-Rubio, C. H. Hendon, J. A. Dumesic and Y. Roman-Leshkov, *Science*, 2016, **352**, 974–978.
- 9 P. Schwach, X. Pan and X. Bao, *Chem. Rev.*, 2017, **117**, 8497–8520.
- 10 T. N. Nguyen, T. T. P. Nhat, K. Takimoto, A. Thakur, S. Nishimura, J. Ohyama, I. Miyazato, L. Takahashi, J. Fujima and K. Takahashi, *ACS Catal.*, 2019, **10**, 921–932.
- 11 L. Wang, L. Tao, M. Xie, G. Xu, J. Huang and Y. Xu, *Catal. Lett.*, 1993, **21**, 35–41.
- 12 D. Wang, J. H. Lunsford and M. P. Rosynek, *J. Catal.*, 1997, **169**, 347–358.
- 13 W. Ding, S. Li, G. D. Meitzner and E. Iglesia, *J. Phys. Chem. B*, 2001, **105**, 506–513.
- 14 T. V. Choudhary, E. Aksoylu and D. W. Goodman, *Catal. Rev. - Sci. Eng.*, 2003, **45**, 151–203.
- 15 A. Puente-Urbina, Z. Pan, V. Paunović, P. Šot, P. Hemberger and J. A. Bokhoven, *Angew. Chem., Int. Ed.*, 2021, **60**, 24002–24007.
- 16 C. Vogt, F. Meirer, M. Monai, E. Groeneveld, D. Ferri, R. A. van Santen, M. Nachtegaal, R. R. Unocic, A. I. Frenkel and B. M. Weckhuysen, *Nat. Commun.*, 2021, **12**, 1–10.
- 17 I. Vollmer, B. Van Der Linden, S. Ould-Chikh, A. Aguilar-Tapia, I. Yarulina, E. Abou-Hamad, Y. G. Sneider, A. I. Olivos Suarez, J. L. Hazemann, F. Kapteijn and J. Gascon, *Chem. Sci.*, 2018, **9**, 4801–4807.
- 18 C. Doornkamp and V. Ponec, *J. Mol. Catal. A: Chem.*, 2000, **162**, 19–32.
- 19 P. Mars and D. W. Van Krevelen, *Chem. Eng. Sci.*, 1954, **3**, 41–59.
- 20 F. Solymosi, J. Cserényi, A. Szöke, T. Bánsági and A. Oszkó, *J. Catal.*, 1997, **165**, 150–161.



- 21 C. Kalha, L. E. Ratcliff, J. G. Moreno, S. Mohr, M. Mantsinen, N. K. Fernando, P. K. Thakur, T.-L. Lee, H.-H. Tseng and T. S. Nunney, *Phys. Rev. B*, 2022, **105**, 045129.
- 22 J. Yang, D. Ma, F. Deng, Q. Luo, M. Zhang, X. Bao and C. Ye, *Chem. Commun.*, 2002, **8**, 3046–3047.
- 23 F. A. L. De Souza, A. R. Ambrozio, E. S. Souza, D. F. Cipriano, W. L. Scopel and J. C. C. Freitas, *J. Phys. Chem. C*, 2016, **120**, 27707–27716.
- 24 A. Laio and M. Parrinello, *Proc. Natl. Acad. Sci. U. S. A.*, 2002, **99**, 12562–12566.
- 25 G. Bussi and D. Branduardi, *Rev. Comput. Chem.*, 2015, **28**, 1–49.
- 26 C. L. Yaws, in *Transport Properties of Chemicals and Hydrocarbons*, Elsevier, 2009, pp. 502–593.
- 27 I. Vollmer, I. Yarulina, F. Kapteijn and J. Gascon, *ChemCatChem*, 2019, **11**, 39–52.
- 28 J. Gao, Y. Zheng, J.-M. Jehng, Y. Tang, I. E. Wachs and S. G. Podkolzin, *Science*, 2015, **348**, 686–690.
- 29 K. Murugappan, E. M. Anderson, D. Teschner, T. E. Jones, K. Skorupska and Y. Román-Leshkov, *Nat. Catal.*, 2018, **1**, 960–967.
- 30 I. Vollmer, N. Kosinov, Á. Szécsényi, G. Li, I. Yarulina, E. Abou-Hamad, A. Gurinov, S. Ould-Chikh, A. Aguilar-Tapia, J.-L. Hazemann, E. Pidko, E. Hensen, F. Kapteijn and J. Gascon, *J. Catal.*, 2019, **370**, 321–331.
- 31 S. K. Kim, H. W. Kim, S. J. Han, S. W. Lee, J. Shin and Y. T. Kim, *Commun. Chem.*, 2020, **3**, 58.
- 32 N. K. Razdan and A. Bhan, *J. Catal.*, 2020, **389**, 667–676.
- 33 A. Barducci, G. Bussi and M. Parrinello, *Phys. Rev. Lett.*, 2008, **100**, 020603.
- 34 A. Barducci, M. Bonomi and M. Parrinello, *Wiley Interdiscip. Rev. Comput. Mol. Sci.*, 2011, **1**, 826–843.
- 35 O. Valsson, P. Tiwary and M. Parrinello, *Annu. Rev. Phys. Chem.*, 2016, **67**, 159–184.
- 36 V. V. Ordonsky, B. Legras, K. Cheng, S. Paul and A. Y. Khodakov, *Catal. Sci. Technol.*, 2015, **5**, 1433–1437.
- 37 L. Q. Huang, Y. Z. Yuan, H. B. Zhang, Z. T. Xiong, J. L. Zeng and G. D. Lin, *Stud. Surf. Sci. Catal.*, 2004, **147**, 565–570.
- 38 T. Zhang, D. Holiharimanana, X. Yang and Q. Ge, *J. Phys. Chem. C*, 2020, **124**(49), 26722–26729.
- 39 J. N. Carstens and A. T. Bell, *J. Catal.*, 1996, **161**, 423–429.
- 40 J. Eng, J. G. Chen, I. M. Abdelrehim and T. E. Madey, *J. Phys. Chem. B*, 1998, **102**, 9687–9696.
- 41 M. Sijaj, H. Oudghiri-Hassani, C. Maltais and P. H. McBreen, *J. Phys. Chem. C*, 2007, **111**, 1725–1732.

